

# Controlling Product Distribution of CO<sub>2</sub> Reduction on CuO-Based Gas Diffusion Electrodes by Manipulating Back Pressure

Baran Sahin,\* Jane J. Leung, Erhard Magori, Steffen Laumen, Angelika Tawil, Elfriede Simon, and Olaf Hinrichsen

The electrochemical reduction reaction of CO<sub>2</sub> (CO<sub>2</sub>RR) is a promising avenue toward the renewable energy-driven transformation of a greenhouse gas toward fuels and value-added chemicals. While copper uniquely can catalyze this reaction to longer carbon chains, Cu-based electrodes continue to face numerous challenges, including low selectivity toward desired products and poor stability. To unlock its potential for large-scale industrial implementation, great interest is shown in tackling these challenges, primarily focusing on catalyst and electrode modifications and thereby leaving a research gap in the effects of operation conditions. Herein, back pressure application is introduced in CO<sub>2</sub> electrolyzers at industrially relevant current densities (200 mA cm<sup>-2</sup>) in order to steer selectivity toward C<sub>2+</sub> products. The back pressure adjusts CO<sub>2</sub> availability at the electrode surface, with a high CO<sub>2</sub> surface coverage achieved at  $\Delta P = 130$  mbar suppressing the competing hydrogen evolving reaction for 72 h and doubling of stable ethylene production duration. Faradaic efficiency of 60% for C<sub>2+</sub> products and overall C<sub>2+</sub> conversion efficiency of 19.8% are achieved with the easily implementable back pressure operation mode presented in this study. It is proven to be a promising tool for product selectivity control in future upscaled Cu-based CO<sub>2</sub> electrolysis cells.

## 1. Introduction


The products of CO<sub>2</sub>RR, such as C<sub>2+</sub> hydrocarbons and alcohols, attract significant global demand. Hori et al.<sup>[1]</sup> discovered in 1985 that Cu is the only metal that can electrochemically reduce CO<sub>2</sub> and CO into significant amounts of hydrocarbons, and since then researchers working in the field of CO<sub>2</sub> electrochemical reduction have to this day continued to focus their efforts on Cu due to its unique ability to convert CO<sub>2</sub> into bigger molecules that require more than two reduction electrons per CO<sub>2</sub> molecule (>2e<sup>-</sup> products).<sup>[2–6]</sup> This special capability of Cu stems from its optimal binding energy for CO<sub>2</sub>RR and hydrogen evolving reaction (HER) intermediates: a negative adsorption energy for CO\*, indicating thermodynamically favorable interaction between components, and a positive adsorption energy for H\*, indicating the opposite.<sup>[6–8]</sup>

Despite these characteristics, electrochemical CO<sub>2</sub>RR on Cu-based electrodes continues to face numerous challenges to its scalability, including product selectivity and stability.<sup>[5,9,10]</sup> Industrially relevant stable operation times (>10 000 h) and high selectivity toward specific value-added products (e.g., ethanol, propanol, or ethylene) at lower potentials are essential for future industrial applications but remain to be achieved. The parasitic HER constitutes one of the main issues, as it over time diverts selectivity toward undesired H<sub>2</sub>, eroding away at stable CO<sub>2</sub>RR operation. Scientists work on different aspects of the CO<sub>2</sub>RR system to overcome these problems: modification of the catalyst structure (morphology,<sup>[11–13]</sup> oxidation state,<sup>[14–16]</sup> facets,<sup>[9,17,18]</sup> grain boundaries<sup>[15]</sup>), application of multiatom catalysts (bimetallic systems,<sup>[2]</sup> tandem catalysts,<sup>[10,19,20]</sup> or dopants<sup>[21,22]</sup>), as well as design of electrode structure.<sup>[23–26]</sup>

Engineering of the electrode structure is a broader aspect that answers to multitudinous facets of the CO<sub>2</sub>RR challenges. In typical aqueous-fed CO<sub>2</sub> electrolyzers (liquid-phase reactors), electrodes suffer from CO<sub>2</sub> mass transport limitations, as CO<sub>2</sub> availability is limited by its solubility in the electrolyte. In gas-fed CO<sub>2</sub> electrolyzers with gas diffusion electrodes (GDEs), the CO<sub>2</sub> solubility problem is eliminated as CO<sub>2</sub> is

B. Sahin, J. J. Leung, E. Magori, S. Laumen, A. Tawil, E. Simon  
Siemens Energy (SE) New Energy Business (NEB) Technology & Products  
(TP) Development (DEV)  
Siemens Energy Global GmbH & Co. KG  
81739 Munich, Germany  
E-mail: baran.sahin@tum.de

B. Sahin, S. Laumen, O. Hinrichsen  
Catalysis Research Center and Chemistry Department  
Technical University of Munich  
85747 Garching b. Munich, Germany

 The ORCID identification number(s) for the author(s) of this article can be found under <https://doi.org/10.1002/ente.202200972>.

© 2022 The Authors. Energy Technology published by Wiley-VCH GmbH. This is an open access article under the terms of the Creative Commons Attribution-NonCommercial-NoDerivs License, which permits use and distribution in any medium, provided the original work is properly cited, the use is non-commercial and no modifications or adaptations are made.

DOI: 10.1002/ente.202200972

transported by gas diffusion to the three-phase boundary where electrolyte, catalyst, and CO<sub>2</sub> coexist. Yet, in cathodes of the GDE type, feed diffusion to the catalyst layer remains the mass transport limiting step. In addition to mass transport, electron and ion transport phenomena are also governed by GDEs. Various parameters can be manipulated to fabricate the optimum GDE, including porosity of diffusion layer, hydrophobicity, thickness of electrode and of catalyst layer, catalyst–diffusion layer interactions, ionomer or binder properties, catalyst–ionomer interactions etc.<sup>[8,23,25]</sup>

The mechanism of CO<sub>2</sub>RR on Cu is a highly debated topic in the literature with various postulated mechanisms for each product.<sup>[4,5,10,27–29]</sup> The product spectrum includes C<sub>1</sub>–C<sub>3</sub> hydrocarbons and oxygenates: carbon monoxide (2e<sup>−</sup>), formate (2e<sup>−</sup>), methanol (6e<sup>−</sup>), methane (8e<sup>−</sup>), acetate (8e<sup>−</sup>), acetaldehyde (10e<sup>−</sup>), ethylene (12e<sup>−</sup>), ethanol (12e<sup>−</sup>), propionaldehyde (16e<sup>−</sup>), allyl alcohol (16e<sup>−</sup>), and n-propanol (18e<sup>−</sup>).<sup>[5]</sup> Half-cell reactions of the main products are listed in Table S1 of the Supporting Information.

Formate and carbon monoxide, C<sub>1</sub> products requiring only 2e<sup>−</sup> electrons for reduction, are typically the first products to be observed at lower (more positive) overpotentials, signaling that their formation demands the lowest kinetic barriers for their formation.<sup>[8]</sup> Adsorbed CO species have been identified in numerous studies as the key intermediate in the reduction of CO<sub>2</sub> to >2e<sup>−</sup> products.<sup>[3,6,10,28,30–35]</sup> Formate is the only product that does not involve a CO\* species as intermediate.<sup>[8,10]</sup> Selectivity between the CO or HCOO<sup>−</sup> pathways is determined by the Cu–C and Cu–O bond strengths. Intermediate species, which are bound either by C or O atom(s) to the catalyst surface, lead to CO and HCOO<sup>−</sup> formation, respectively.<sup>[8]</sup> The other common C<sub>1</sub> product, methane, is formed from CO\* with a series of electron–proton transfers, requiring 8e<sup>−</sup> for its reduction from CO<sub>2</sub>.<sup>[5,8,36]</sup>

C<sub>2+</sub> product mechanisms must include C–C coupling step(s), necessitating two adjacent C-containing adsorbates. Ethylene is formed via dimerization of two CO adsorbed species and its further reduction to the alkene form.<sup>[5,6,17,27,33,37]</sup> Ethanol and ethylene pathways differentiate from one another, where hydrogenation of \*CHCOH leads to the former and deoxidation of a hydroxyl group in \*CHCOH to the latter.<sup>[33,38]</sup> Acetaldehyde is suggested as an intermediate species in the ethanol formation mechanism.<sup>[3,28,39–41]</sup> Another C<sub>2+</sub> product, acetate's formation mechanism, is not yet agreed upon in the literature. There are studies claiming that homogeneous chemical reactions in alkaline electrolytes resulting from OH<sup>−</sup> attack on a surface-bound ketene or other carbonyl-containing intermediate (Cannizzaro-type disproportionation) after C–C coupling leads to acetate formation.<sup>[15,42]</sup> C<sub>3</sub> alcohol is possibly formed with a selective C–C coupling of \*C<sub>1</sub> and \*C<sub>2</sub> intermediates that result in propionaldehyde formation and it is followed by rapid hydrogenation to C<sub>3</sub> alcohol.<sup>[28,41,43,44]</sup>

The presence of various possible surface species and their coverage as defined by the applied potential makes C–C coupling a potential-dependent phenomenon.<sup>[5]</sup> Higher cathodic potentials are required to permit C–C coupling reactions.<sup>[34,43,45]</sup> In concordance with this requirement, it is proposed that C<sub>2</sub> pathways necessitate a lowered activation energy of CO–CO dimerization,<sup>[33]</sup> which is the rate-determining step for C<sub>2</sub> pathways according to the literature.<sup>[27,46–48]</sup> The rate of C<sub>2+</sub> formation is therefore determined by the rate of conversion of adsorbed CO\* species to the

C<sub>2+</sub> product, assuming sufficient coverage of the key intermediate CO\*.<sup>[37]</sup> The selectivity toward oxygenated products is higher at more positive onset potentials due to the weaker driving force for polarizing C–O-containing intermediates. As a result, the C–O bond remains and it leads to oxygenate products.<sup>[3]</sup>

Among Cu-based CO<sub>2</sub>RR catalysts, oxide-derived Cu draws special attention owing to its better selectivity, stability, and energy efficiency. Oxide-derived Cu compared with metallic Cu possesses more porous surfaces<sup>[8]</sup> with undercoordinated sites formed by special grain boundary terminations,<sup>[8,19,43,49]</sup> enabling high selectivity toward oxygenates at relatively low overpotentials.<sup>[3,15,19,40,50–52]</sup> In situ reduction of Cu oxides in the cathode under electrolysis conditions alters the crystal morphology, which has been shown to change the catalyst's selectivity and stability.<sup>[3,12,16,36]</sup>

Cu-based electrodes' activity toward CO<sub>2</sub>RR notoriously decay over time, posing the greatest obstacle for its commercialization. There are various hypotheses about the origin of this. Hori et al.<sup>[53]</sup> suggested deposition of metallic impurities as the cause of catalyst poisoning, whereas more recent studies claim impurity poisoning occurs only with very small electrode sizes<sup>[8,36]</sup> or result from C\* surface species that can be formed as a reaction intermediate in the C<sub>1</sub> pathway.<sup>[30,31,43,54–58]</sup> CO<sub>2</sub>RR instability is also attributed to surface reconstruction by both sintering and declustering at different time periods of the electrolysis.<sup>[59]</sup> In addition to catalyst-related phenomena, limitation of CO<sub>2</sub> availability (e.g., by electrode flooding) on the electrode surface can compromise CO<sub>2</sub>RR stability. Several studies suggest that flooding of GDEs is the key way in which electrolytes create CO<sub>2</sub>-depleted zones, leading to the dominance of HER.<sup>[60–62]</sup>

Among other operational parameters, pressure has a unique role in CO<sub>2</sub>RR as it has a threefold effect: capillary effects on the electrode flooding, mechanical effects providing better contact between electrolysis cell components, and increase in CO<sub>2</sub> concentration in the gas phase and therefore the CO<sub>2</sub>\* surface coverage on the catalyst. By means other than manipulating pressure, researchers have controlled CO<sub>x</sub>\* coverage on the electrode surface by manipulating CO<sub>2</sub> or CO feed concentration. Lie et al.<sup>[46]</sup> diluted the CO feed and Tan et al.<sup>[63]</sup> the CO<sub>2</sub> feed with N<sub>2</sub> to study their coverage effects. Applying an impulse current is another technique to control local CO<sub>2</sub> concentration by enabling transient conditions of high local CO<sub>2</sub> concentration.<sup>[64,65]</sup>

In this work, we have employed a different approach, by varying the back pressure of the gas side in the electrolyzer to manipulate CO<sub>2</sub>\* coverage on the electrode surface and minimize flooding effects. We show that back pressure as an operation parameter in CO<sub>2</sub>RR can be manipulated to control product selectivity and improve stability of the electrodes. With applied back pressure of 0–130 mbar between the gas side of the electrochemical cell and catholyte chamber, we demonstrate that the Faradaic efficiency (FE) for desired C<sub>2+</sub> products is improved up to 60% at 200 mA cm<sup>−2</sup> and that stable operation of CO<sub>2</sub>RR is maintained for more than 72 h, during which HER is successfully suppressed to below 25% FE (at 130 mbar). C<sub>2+</sub> conversion efficiency for CO<sub>2</sub>RR products reaches up to 19.8%. Our results prove that back pressure may be manipulated in future upscaled CO<sub>2</sub>RR systems with CuO-based GDEs to control the product selectivity and improve the CO<sub>2</sub>RR stability.

## 2. Experimental Section

### 2.1. Electrode Preparation

CuO powder particles delivered by Johnson Matthey were used for the preparation of Cu-based GDEs. A CuO ink was prepared with 40 mg of CuO powder, 160 mg of 5 wt% Sustanion XA-9 anionic ionomer in ethanol solution, and 4 mL of isopropanol (99.9%, Sigma Aldrich). The ink was sonicated in an ultrasonic water bath for 30 min and immediately drop cast onto a 10 cm × 5.5 cm carbon-based gas diffusion layer (GDL) from Freudenberg (H23C2), which consisted of two layers: a carbon-based microporous layer containing hydrophobic PTFE binder and a macroporous layer consisting of carbon fibers. Together with the drop-cast catalyst layer, the GDE therefore had three layers. Later, the electrode was dried overnight at room temperature under a N<sub>2</sub> atmosphere with a flow of 50 sccm. The dried electrode batch was cut into two pieces with a 48 mm × 44 mm cutting template. The active area that took part in the electrolysis was 10 cm<sup>2</sup>. The catalyst loading was 0.73 mg cm<sup>-2</sup>.

### 2.2. Electrode Surface Analysis

A Bruker D2 PHASER diffractometer (Cu K radiation, scan rate of 0.02° s<sup>-1</sup>) was used to perform ex situ X-ray diffraction (XRD) analysis on electrodes pre- and postelectrolysis. Scanning electron micrographs (SEM) of the GDEs pre- and postelectrolysis were taken at different magnifications with a high-resolution field-emission scanning electron microscope (JSM-7500F, JEOL). Both XRD and SEM results are given in the Supporting Information.

### 2.3. Experimental Set-Up

An internally designed flow cell was used in all experiments (Figure S5 and S6, Supporting Information). The cell consisted of three compartments where gas, catholyte, and anolyte flow in and out, respectively. PTFE and PEEK materials were used to determine the fluid flow patterns, to ensure cell tightness and provide better mechanical stability for the GDE and membrane. An IrO<sub>x</sub>-coated electrode with a 10 cm<sup>2</sup> active area (Electrocell) was used as the anode and the CuO GDE described above as the cathode. Anode and cathode chambers were separated from one another by a cation exchange membrane (CEM) (Nafion 117, Ion Power). 250 mL of 1 M KHCO<sub>3</sub> (+99.7% in dry basis, Alfa Aesar) was circulated in the system as electrolyte between the gaps of cathode–membrane (catholyte) and anode–membrane (anolyte). The electrolyte flows circulating in both anode and cathode gaps were mixed in an electrolyte chamber external to the cell and pumped continuously through the system with microdiaphragm liquid pumps (NFB 25 KPDCB-4A, KNF) operated at a constant flow of 100 mL min<sup>-1</sup>. The gas chamber was fed with CO<sub>2</sub> (+99.998%, Linde) which was humidified by a custom-made water bubbler at room temperature. Gas flow rates in the system were controlled with mass flow controllers (SFC5400 Sensirion). In contrast to the electrolyte, the gas head spaces of catholyte and anolyte were kept separate. The gas outlet from the cell was

mixed with catholyte head space. The setup and cell details are shown in the Supporting Information.

### 2.4. Electrochemical Measurements

Chronopotentiometric electrochemical measurements were performed at 200 mA cm<sup>-2</sup> (2 A) using a Bio-Logic VSP 3e potentiostat, controlled by the EC-Lab software. Ag/AgCl (3 M NaCl) was used as the reference electrode (RE). Control experiments (Base case at Δ*P* = 0) were conducted without a back pressure valve, whereas back pressure was applied, as shown in **Figure 1**, for the back pressure experiments. Feed flow rate variation was based on the λ value, and simply the ratio of actual CO<sub>2</sub> flow rate to the CO<sub>2</sub> flow rate theoretically required for full utilization of electrons to ethylene formation, formulated in Equation (2), where  $\dot{V}$  is the flow rate, *F* is the Faraday constant, *I* is the applied current, *z* is the number of electrons required for the reduction, *t* is the electrolysis time, *R* is the ideal gas constant, *T* is the temperature, and *P* is gas pressure.

$$\lambda = \frac{\dot{V}_{\text{CO}_2, \text{actual}}}{\dot{V}_{\text{CO}_2, \text{theoretical}}} = \frac{\dot{V}_{\text{CO}_2, \text{actual}}}{2 \times \frac{I \times t}{z \times F} \times \frac{R \times T}{P}} \quad (1)$$

C<sub>2+</sub> conversion efficiency is defined as the ratio of the molar sum of the converted CO<sub>2</sub> into C<sub>2+</sub> products to the CO<sub>2</sub> feed into the electrolyzer in moles, as expressed in Equation (3), where θ<sub>*i*</sub> is the number of carbons in the product *i*,  $\dot{n}_i$  is the produced amount of product *i* in moles, and  $\dot{n}_{\text{CO}_2, \text{feed}}$  is the molar amount of fed CO<sub>2</sub>.

$$\text{C}_{2+} \text{ conversion efficiency} = \frac{\sum \theta_i \times \dot{n}_i}{\dot{n}_{\text{CO}_2, \text{feed}}} \quad (2)$$

Electrochemical impedance spectroscopy (EIS) measurements were performed to determine cell resistance. Cell resistance, *R*, was used in the calculation of *iR* in order to correct the working electrode potential. High-frequency resistance obtained from EIS measurements corresponded to cell resistance and accounted for 0.34 Ω. *iR*-corrected working electrode potential corresponded to −0.79 V versus RHE. The potentials, recorded versus the RE, were converted to the reversible hydrogen electrode (RHE) scale according to the Nernst equation.

$$V \text{ vs. RHE} = V_{\text{measured vs. Ag/AgCl}} + 0.209 + 0.059 \times \text{pH} \quad (3)$$

### 2.5. Product Analysis

The catholyte gas head space was connected to a gas chromatograph (GC) for quantitative product analysis (7890B Agilent, Santa Clara, USA). N<sub>2</sub> was mixed with the product stream before the GC inlet as an internal standard for quantification. He is the carrier gas enabling the detection of H<sub>2</sub> as a negative peak. A thermal conductivity detector (TCD) and three serially connected columns were used: a HayeSeP Q-column, a Porapak Q-column for the separation of CH<sub>4</sub>, CO<sub>2</sub>, and C<sub>2</sub>H<sub>4</sub>, and a molecular sieve 5 Å column to separate N<sub>2</sub>, O<sub>2</sub>, and CO. 1 mL of the gas product

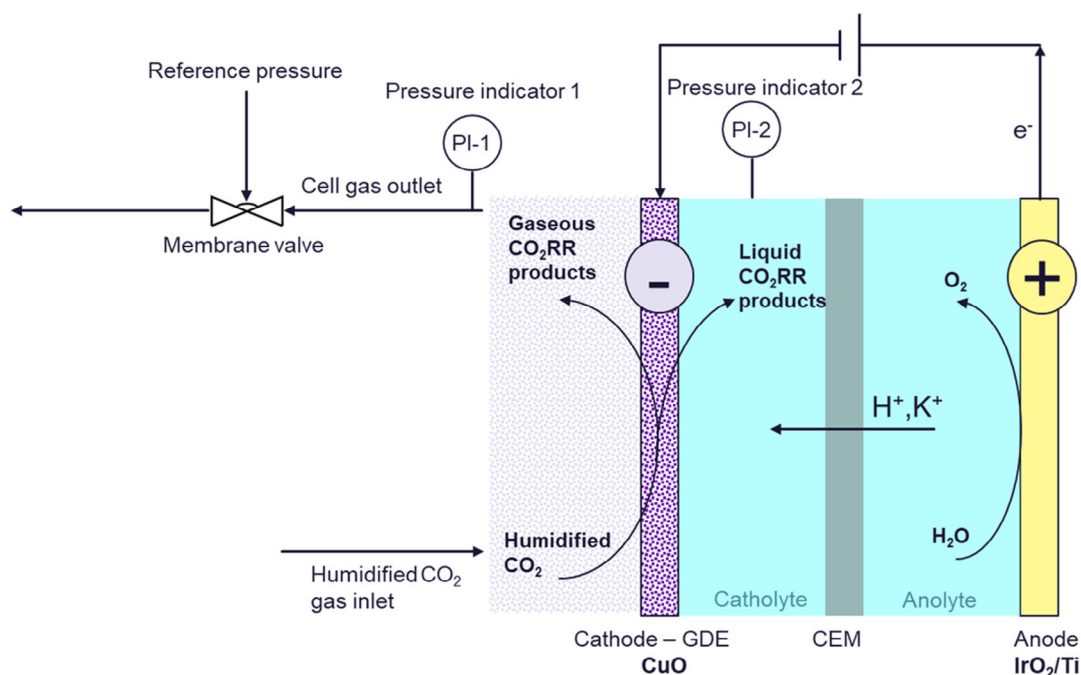


**Figure 1.** Experimental setup for CO<sub>2</sub>RR in flow cell architecture with back pressure application at the gas side.

stream was automatically injected every 20 min from the cell to the GC during the course of the electrolysis.

<sup>1</sup>H nuclear magnetic resonance (NMR) was used for quantification of liquid products. Electrolyte circulated constantly in a separated closed system between reservoir and cell sampled from a septum. The NMR measurements were performed in a 500 MHz Bruker (Bruker Bio-Spin, Karlsruhe, Germany) following the method described by Cuellar et al.<sup>[45]</sup> The water peak was suppressed by a presaturation sequence. An aliquot of the KHCO<sub>3</sub> electrolyte-containing liquid products (300 μL) was mixed with sodium fumarate as an internal standard (50 μL) in D<sub>2</sub>O (250 μL) for quantification.

FEs corresponding to gas and liquid products are calculated using the following equation, where *n* is the amount of product in moles

$$FE = \frac{n \times z \times F}{I \times t} \quad (4)$$

### 3. Results and Discussion

The setups for CO<sub>2</sub>RR with back pressure operation and experimental results are explained in three main categories: cell setup, stability under back pressure, product selectivities under different back pressure values, and flow rates. The characterization of the electrodes is presented in Supporting Information.

#### 3.1. Cell Setup and Application of Back Pressure

Back pressure experiments were performed on carbon-based GDEs embedded with a commercial CuO catalyst, positioned

in a two-gap flow cell architecture (see Experimental Section and Figure S1–S4, Supporting Information, for electrode description and characterization). The cells consist of two electrodes separated by a CEM and two gaps that accommodate electrolyte flow (1 M KHCO<sub>3</sub>, flow rate = 100 mL min<sup>-1</sup>; Figure 1). The third compartment, namely, the gas chamber where humidified CO<sub>2</sub> (atmospheric gas inlet pressure) flows, comes into contact only with the cathode and therefore does not reside between the two conductive electrodes. A membrane valve is positioned at the gas outlet stream that carries mainly unconverted CO<sub>2</sub>, H<sub>2</sub>, and CO<sub>2</sub>RR gas products. The absolute pressure in the gas compartment is increased and controlled by the membrane valve.

Pressures in the gas compartment and in the catholyte chamber were monitored with pressure sensors. The back pressure ( $\Delta P$ ) applied on the GDE is defined as the difference between *P*<sub>1</sub> (gas) and *P*<sub>2</sub> (catholyte). This was set to 70 and 130 mbar at high gas flow rates and 40 mbar in low-gas flow rate experiments. It must be noted that higher back pressures can lead to so-called “flow-through” operation, where the pressure difference enables the gas to be pushed through the porous electrode to the catholyte chamber on the other side. For this reason, back pressure must be set to a value that maintains the desired “low-by” operation. This threshold value for flow-by strongly depends on the electrode architecture and properties, employed flow rate, catholyte properties, and cell design and size. We stress that optimum back pressure values can vary in differing cell systems and should therefore be optimized accordingly.

#### 3.2. HER Suppression Under Back Pressure

The stability of the CuO electrodes was tested at an applied current density of 200 mA cm<sup>-2</sup> in two series of experiments: base

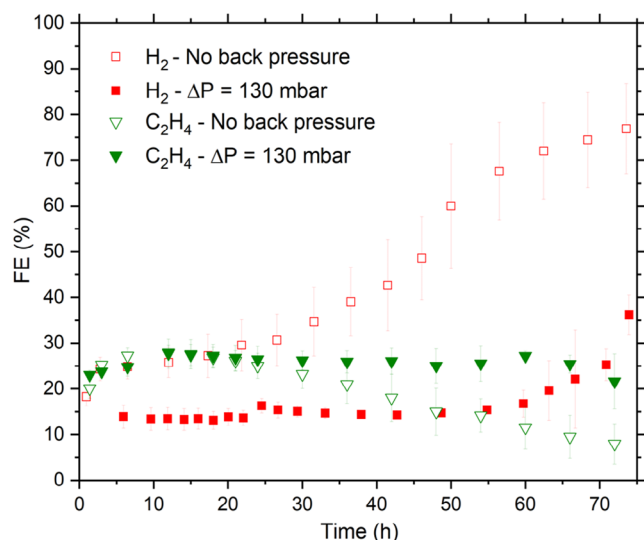


**Figure 2.** Stability of the CO<sub>2</sub> electrolysis system expressed in terms of hydrogen and ethylene faradaic efficiencies.

case without back pressure and with  $\Delta P = 130$  mbar. In **Figure 2**, the FE for H<sub>2</sub> and C<sub>2</sub>H<sub>4</sub> is depicted versus time for both cases. HER as the competing reaction to CO<sub>2</sub>RR is a good indicator for a decrease in CO<sub>2</sub>RR catalytic activity. FE<sub>C<sub>2</sub>H<sub>4</sub></sub> is chosen as an indicator of CO<sub>2</sub>RR stability, as it is one of the more valuable CO<sub>2</sub>RR products. At a back pressure of 130 mbar, FE<sub>H<sub>2</sub></sub> is suppressed below 25% for 72 h, in comparison with the base case where H<sub>2</sub> selectivity is clearly higher already from the outset at 25–40% for the first 48 h and only becomes more dominant over time (FE<sub>HER</sub> > 50%). Two separate phenomena are observed here: 1) Back pressure significantly decreases the selectivity for H<sub>2</sub>. At 24 h, FE<sub>HER</sub> is 15.1 (±1.0)% under  $\Delta P = 130$  mbar, whereas in the base case it is almost double this at 30.7 (±5.6)% in the base case; and 2) Back pressure provides longer stable CO<sub>2</sub>RR operation. FE<sub>C<sub>2</sub>H<sub>4</sub></sub> remained above 20% for only 36 h in the base case, while back pressure of 130 mbar prolonged its stability to 72 h, corresponding to a stability increase by a factor of two when 20% is assumed as the stability threshold.

The two above phenomena must be regarded separately. Regarding the first, it has been suggested that abundant CO\* coverage on Cu suppresses HER due to site-blocking effects and/or changes in H\* binding energy, leading to higher FEs for CO<sub>x</sub>RR.<sup>[6,15,30,43,58,66,67]</sup> The surface coverage of CO<sub>2</sub>\* on the catalyst is dependent on the local concentration of CO<sub>2</sub>, as per Equation (5), where  $\theta^*$  is the coverage of vacant surface sites,  $E$  is the CO<sub>2</sub> adsorption energy on the surface,  $R$  is the ideal gas constant, and  $T$  is the temperature.

$$\theta_{\text{CO}_2} = \theta^* \times [\text{CO}_2] \times e^{\frac{-E}{RT}} \quad (5)$$

According to the adsorption equilibrium equation, adsorbed CO<sub>2</sub> species coverage (CO<sub>2</sub>\*) increases with increasing CO<sub>2</sub> concentration in the gas phase, assuming that CO<sub>2</sub> adsorption is molecular and first order.<sup>[46,63]</sup> **Figure 3** schematically illustrates the increasing surface coverage of CO<sub>2</sub>\* with increasing partial pressure of CO<sub>2</sub> provided by application of back pressure. As

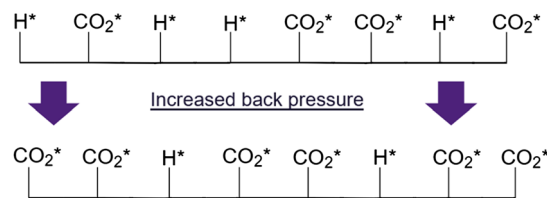


**Figure 3.** Simplified illustration of catalyst surface coverage of CO<sub>2</sub>\* and H\* species under back pressure.

CO<sub>2</sub> adsorption (CO<sub>2</sub> → CO<sub>2</sub>\*) is the rate-determining step of CO<sub>2</sub> reduction to <2e<sup>-</sup> products and the reaction from CO<sub>2</sub>\* to CO\* is faster, a higher CO<sub>2</sub> partial pressure would accordingly translate into an abundant CO\* surface coverage.<sup>[8]</sup> Based on our results, it can be assumed that increased back pressure leads to higher CO\* coverage and therefore HER suppression.

On the second phenomenon, two explanations for longer stability under back pressure are possible. As mentioned, catalysts producing more C<sub>2+</sub> relative to C<sub>1</sub> products may be more stable due to a possible graphitic intermediate in the C<sub>1</sub> route.<sup>[35,36,47,59–63]</sup> In mechanistic studies conducted by Rahaman et al.<sup>[43]</sup> and Akhade et al.,<sup>[58]</sup> the poisoning C\* species is postulated to be formed via reduction of COH\*, which is an intermediate of CO\*-to-CH<sub>4</sub> reduction. As discussed in the following subsections, abundant CO\* coverage provided by back pressure suppresses C<sub>1</sub> hydrocarbon production (CH<sub>4</sub>) and promotes C<sub>2+</sub> selectivity. This may have resulted in the observed longer stability by avoiding poisonous C\* intermediate formation, as this route is not preferred under high CO\* coverage. Another possibility is that back pressure keeps the capillary pressure (local pressure difference between wetting and nonwetting media) at a sufficiently high value that minimizes the flooding of the catalyst and GDLs, an otherwise highly likely cause of deactivation.<sup>[60–62]</sup> When flooding is minimized, the salts present in the aqueous electrolyte do not crystallize in the pores of the electrode and do not increase its hydrophilicity. We hypothesize that flooding occurs to a smaller degree or can be delayed under back pressure. Mass transport limitation on CO<sub>2</sub> availability therefore remains low and can be avoided for a longer period.

### 3.3. C<sub>1</sub> Product Formation under Back Pressure

FEs of three main C<sub>1</sub> products, CO, COOH<sup>-</sup>, and CH<sub>4</sub>, obtained under CO<sub>2</sub>RR conditions at an applied current density of 200 mA cm<sup>-2</sup> and at three different back pressure conditions are shown in **Figure 4**. Methanol is detected only in trace amounts and has not been included in the results.

The key intermediate CO is produced in significantly larger amounts when back pressure is applied, indicating that CO\* desorbs before being reduced further to >2e<sup>-</sup> products. FE<sub>CO</sub> = 18.3 ± 0.6% in the base case compared with 26.0 ± 2.1% under 70 mbar and 26.7 ± 1.8% under 130 mbar back pressure. Therefore, a correlation between increasing back pressure and CO desorption may be established. A similar trend of increased CO production at higher pressures is described in the literature, the cause of which is given as the increased CO\* surface coverage under higher pressures.<sup>[36,43,63]</sup> It has also been

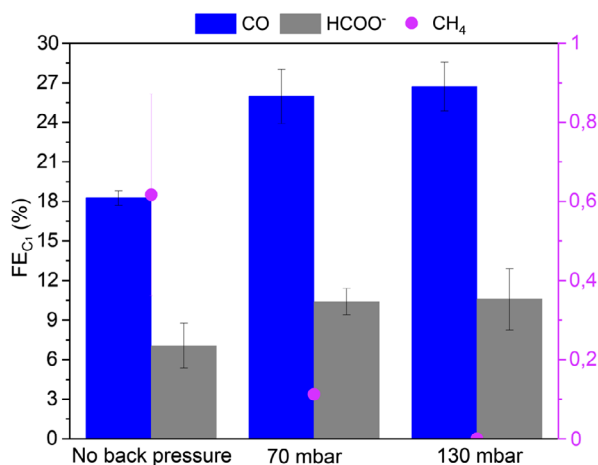


**Figure 4.** C<sub>1</sub> product distribution dependency on back pressure at t = 3 h.

claimed that abundant CO<sub>2</sub>\* coverage reduces the CO\* binding energy to the catalyst surface via adsorbate–adsorbate repulsion, which, in turn, causes CO to bond weakly and therefore its desorption.<sup>[68]</sup> Additionally, we hypothesize that shorter residence times due to a stronger driving force for diffusion through the catalyst layer at higher back pressures deprive CO<sub>2</sub> of sufficient residence time to react to >2e<sup>-</sup> products.

The production of formate, the only product that is formed exclusively from CO<sub>2</sub>\* and not through CO\*, is also slightly greater under back pressure, enhanced by the higher CO<sub>2</sub>\* surface coverage under such conditions. Notably, this increase in FE<sub>HCOOH<sup>-</sup></sub> is not as high as that of CO. This might suggest that the proportion of CO<sub>2</sub> atoms bound to the Cu surface via the C atom (leading to CO pathways) becomes significantly higher under back pressure, whereas the number of CO<sub>2</sub> atoms bound to Cu surface by O atom(s) (leading to HCOO<sup>-</sup> pathway) does not increase as much.

FE for CH<sub>4</sub> is observed to decrease from 0.6% in the base case, to 0.1% at 70 mbar back pressure and to 0% at 130 mbar back pressure. The lower selectivity toward CH<sub>4</sub> in the base case can be attributed to the intrinsic catalytic behavior of CuO. Oxide-derived Cu catalysts are known to demonstrate low selectivities for CH<sub>4</sub><sup>[43,69]</sup> and the presence of several Cu<sub>2</sub>O facets is proven to diminish methane formation.<sup>[43]</sup> The gradual decrease of FE<sub>CH<sub>4</sub></sub> with increasing back pressure and the complete suppression of CH<sub>4</sub> at 130 mbar may be correlated to abundant CO<sub>2</sub>\* coverage, which prohibits H\* surface coverage and therefore protonation of CO\* intermediates required for CH<sub>4</sub> formation.

### 3.4. C<sub>2+</sub> Product Formation under Back Pressure

C<sub>2+</sub> products from CO<sub>2</sub>RR on Cu surfaces typically possess either 2 or 3 carbon atoms. It is logical to divide >2e<sup>-</sup> CO<sub>2</sub>RR products into two groups as hydrocarbons and oxygenates as they follow distinct potential dependencies, mechanistic pathways, and surface coverage dependencies. Ethylene and methane constitute the hydrocarbons group whereas methanol, ethanol, n-propanol, allyl alcohol, acetaldehyde, propionaldehyde,

and acetate constitute the oxygenates group. Ethylene is categorized separately from the others as it is the only C<sub>2+</sub> hydrocarbon molecule, the rest being oxygenates. Acetaldehyde, propionaldehyde, and propionate are detected only in trace amounts and have not been included in the results, while allyl alcohol and acetate are observed in very small amounts and have been included within the C<sub>2+</sub> and oxygenate groups.

FE<sub>C<sub>2</sub>H<sub>4</sub></sub> does not change significantly at different back pressure levels and accounts for ≈23–25% in all cases (Figure 5a). FE for total C<sub>2+</sub> products is however enhanced from 36.9% in the base case to 43.0% at ΔP = 70 mbar and 43.9% at ΔP = 130 mbar, and clearly stems not from ethylene but rather from oxygenate formation (Figure 5b). The ratio of >2e<sup>-</sup> oxygenates to hydrocarbons can be tuned between 0.53 and 0.85 at 0 < ΔP < 130 mbar. An enhancement of FE<sub>Oxygenates</sub> from 13% to 20% (accounting for an improvement of 54% in oxygenate selectivity) is driven mainly by ethanol and propanol formation and can be achieved simply by varying the back pressure.

The observed correlation between back pressure and C<sub>2+</sub> selectivity can be explained with the predicted second-order

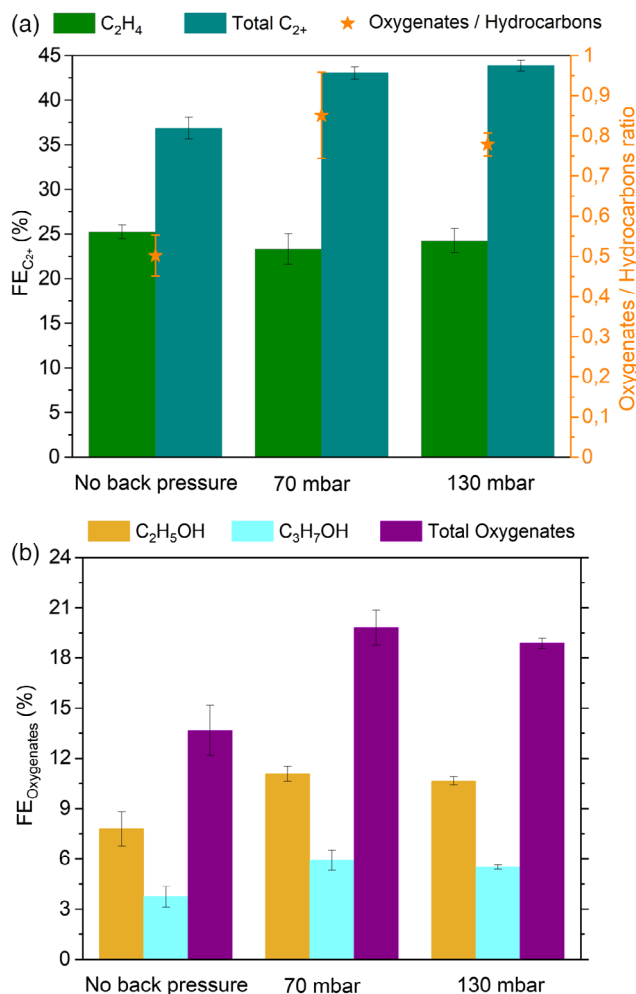


**Figure 5.** a) C<sub>2</sub>H<sub>4</sub> and C<sub>2+</sub> production under back pressure expressed in terms of FE and the ratio of FE sums of oxygenates to hydrocarbons at t = 3 h. b) FEs of oxygenate products at t = 3 h.

kinetic dependency of CO\* coverage for C–C coupling,<sup>[37]</sup> leading to accelerated C<sub>2+</sub> production kinetics with higher CO\* coverage. Nevertheless, we do not exclude the effect of possible changes in local pH when local CO<sub>2</sub> concentrations are higher due to back pressure. The selectivity between ethylene and oxygenates may be explained by the effects of high CO\* coverage on the reaction mechanism, as Li et al. discussed with both density functional theory calculations and experimentation:<sup>[46]</sup> \*CHCOH intermediates tendentially deoxidize to \*CCH under lower CO\* coverage, leading to the ethylene reaction pathway versus tending to hydrogenate to \*CHCHOH under higher CO\* coverage and hence the oxygenate pathway. Our experimental results confirm this. Oxygenate selectivity improvements (and correspondingly improved C<sub>2+</sub> selectivity) achieved with higher CO<sub>2</sub> or CO feed concentrations have similarly been reported by others.<sup>[3,15,51]</sup> We therefore demonstrate that such trends may also be influenced by applying a back pressure.

In parallel with the aforementioned stability of C<sub>2</sub>H<sub>4</sub> formation, FE<sub>C<sub>2+</sub></sub> drops only minimally from 43.9% to 40.5% between the 3rd and 48th h of electrolysis when under ΔP = 130 mbar. In stark contrast to this, FE<sub>C<sub>2+</sub></sub> diminishes drastically from 36.9 to 22.8% within same period if no back pressure is applied. A detailed breakdown of product selectivities over time is given in Table S4, Supporting Information.

### 3.5. Deconvolution of Back Pressure Effects on Stability and Selectivity

Control of CO<sub>2</sub> coverage over catalyst surface and capillary pressure control circumventing the electrode flooding have been mentioned as the possible underlying reasons of the stability and selectivity effects of back pressure application. To decouple these two phenomena from each other, two various experiment series both with ΔP = 130 mbar (P<sub>abs</sub> = 1.13) back pressure application at different two different feed compositions were performed: 100% CO<sub>2</sub> feed (P<sub>CO<sub>2</sub></sub> = 1.13 bar) and CO<sub>2</sub>: N<sub>2</sub> feed in volumetric ratio of 88.5:11.5 (P<sub>CO<sub>2</sub></sub> = 1.00 bar). The diluted feed experiments with ΔP = 130 mbar have the same CO<sub>2</sub> partial pressure of 1.00 bar as the control experiments with no back pressure in the base case (P<sub>abs</sub> = 1 bar, P<sub>CO<sub>2</sub></sub> = 1 bar).

C<sub>2</sub>H<sub>4</sub> and H<sub>2</sub> FEs over time are shown as the stability indicators in **Figure 6**. N<sub>2</sub>-diluted CO<sub>2</sub>-fed experiments at ΔP = 130 mbar exhibit C<sub>2</sub>H<sub>4</sub> stability for ≈48 h, almost identically to the base case with no back pressure. It is significantly inferior to the 72 h stability of pure CO<sub>2</sub>-fed experiments at ΔP = 130 mbar. H<sub>2</sub> was not as suppressed with P<sub>CO<sub>2</sub></sub> = 1.00 bar as it was with P<sub>CO<sub>2</sub></sub> = 1.13 bar, its FE was on constant rise after 48 h, similar to the base case with no back pressure. In the light of these results, back pressure can provide H<sub>2</sub> suppression and stable C<sub>2</sub>H<sub>4</sub> formation primarily by means of increased CO<sub>2</sub> coverage and not necessarily through capillary pressure preventing electrolyte incorporation into the catalyst layer, as the same ΔP = 130 mbar with diluted CO<sub>2</sub> feed could not maintain stable C<sub>2</sub>H<sub>4</sub> formation and H<sub>2</sub> suppression.

**Figure 7** sets out the effects of P<sub>CO<sub>2</sub></sub> on product distribution under the same back pressure of ΔP = 130 mbar. CO selectivity did not differ significantly and failure of H<sub>2</sub> suppression at P<sub>CO<sub>2</sub></sub> = 1.00 bar was discussed thoroughly above. FE<sub>C<sub>2</sub>H<sub>4</sub></sub> was

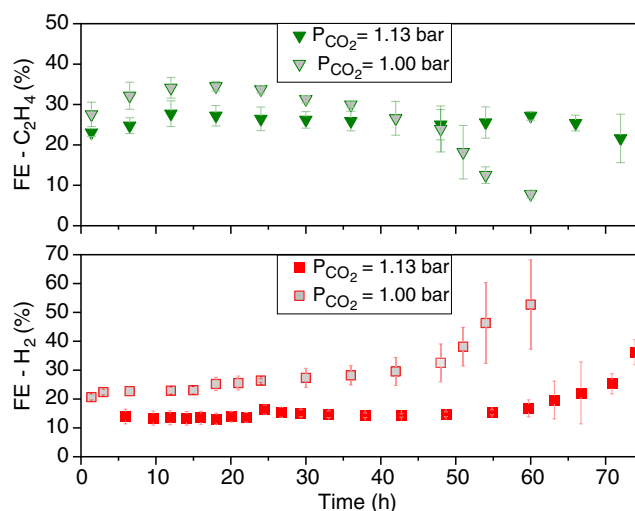


**Figure 6.** Faradaic efficiencies of C<sub>2</sub>H<sub>4</sub> and H<sub>2</sub> over time with 1.13 and 1.00 bar of CO<sub>2</sub> partial pressures under ΔP = 130 mbar back pressure applications.

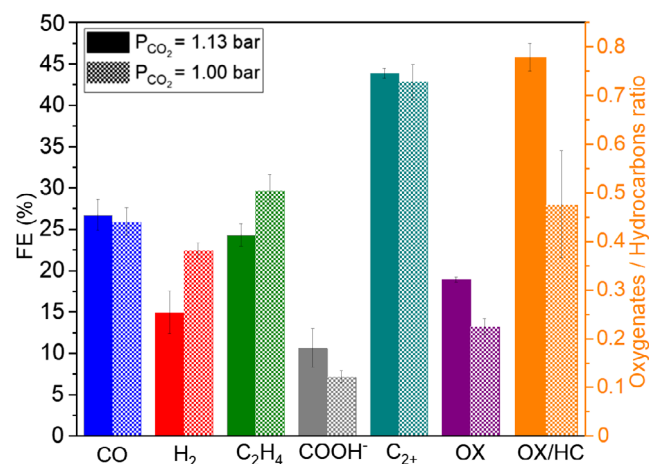


**Figure 7.** Product distributions with 1.13 and 1.00 bar of CO<sub>2</sub> partial pressures under ΔP = 130 mbar back pressure applications at t = 3 h.

greater at P<sub>CO<sub>2</sub></sub> = 1.00 bar with diluted CO<sub>2</sub> feed (29.6%) compared to the P<sub>CO<sub>2</sub></sub> = 1.13 bar case (24.3%). COOH<sup>−</sup> was formed substantially in smaller amounts at lower P<sub>CO<sub>2</sub></sub>. Oxygenate selectivity was significantly improved at higher P<sub>CO<sub>2</sub></sub>. In line with the previous findings, we confirm that high CO<sub>2</sub> coverage at P<sub>CO<sub>2</sub></sub> = 1.13 bar promotes COOH<sup>−</sup> and oxygenate selectivities. P<sub>CO<sub>2</sub></sub> = 1.00 bar condition with diluted CO<sub>2</sub> feed (88.5 vol%) possibly enabled a milder CO<sub>2</sub>, shifting the oxygenate–hydrocarbon (C<sub>2</sub>H<sub>4</sub>) selectivity toward the hydrocarbon.

Base case experiments (P<sub>abs</sub> = 1 bar) and dilute CO<sub>2</sub> feed experiments at ΔP = 130 mbar back pressure (P<sub>abs</sub> = 1.13 bar), both employing P<sub>CO<sub>2</sub></sub> = 1 bar, showed similar product distribution (Figure S8, Supporting Information). The slight differences favoring CO and C<sub>2</sub>H<sub>4</sub> over H<sub>2</sub> in the dilute CO<sub>2</sub> feed at ΔP = 130 mbar may be attributed to the prevention of electrolyte

incorporation to the catalyst layer by the presence of back pressure.

### 3.6. Combined Effect of Back Pressure and Low Flow Rates

Despite the improvements obtained in terms of stability and selectivity toward  $C_{2+}$ , oxygenates through back pressure applications, the increase observed in CO production remains (Figure 4) and limits the overall selectivity for  $C_{2+}$  that can be achieved as it implies lost opportunity for its further reduction. Additionally, improved  $C_2H_4$  selectivity has not been achieved despite abundant surface coverage of  $CO_2^*$  provided by back pressure.

Shorter residence times at the catalyst-coated surface of the electrode is a possible reason for the above observations. A series of experiments at a lower  $CO_2$  feed flow rate were conducted to investigate whether a further reduction of  $CO^*$  may be achieved by a longer residence time and a more optimum surface coverage for  $C_2H_4$ . Feed flow rates are expressed in terms of  $\lambda$ , which is the ratio of actual  $CO_2$  flow rate to the  $CO_2$  flow rate theoretically required for full utilization of electrons for ethylene formation ( $FE_{C_2H_4} = 100\%$ ; see Equation (2) in the Experimental Section). A  $CO_2$  feed of 50 sccm, equivalent to  $\lambda = 10.78$ , is supplied for high flow rate experiments and 14 sccm  $CO_2$ , equivalent to  $\lambda = 3.01$ , is fed to the electrolyzer for low flow rate experiments.  $CO_2RR$  was conducted under four different conditions: high flow rate experiments under  $\Delta P = 130$  and 0 mbar back pressure and low flow rate experiments under  $\Delta P = 40$  and 0 mbar back pressure. The back pressures applied in each of these flow rate conditions correspond to the maximum achievable back pressure if a flow-by operation were to be maintained; a pressure difference exceeding these values for the two cases caused flow-through operation. It is worth noting that the maximum achievable back pressure for flow-by operation strongly depends on electrode characteristics, cell design, catholyte wetting properties and gas flow rate, and the values reported here are therefore highly specific to the experimental materials and design employed.

It is important to emphasize that  $CO_2$  availability in the catalyst layer of the electrode changes fundamentally under low flow rate conditions. The bulk  $CO_2$  gas concentration is reduced from 81.9 to 33.3 mol%, when  $CO_2$  is fed into the electrolyzer cell inlet at 50 and 14 sccm, respectively (see Table S2, Supporting Information). The local  $CO_2$  gas concentration at the catalyst is predicted to be even lower in the low  $\lambda$  case, as a thicker gas boundary layer with higher mass transfer resistance can be expected. Therefore, the difference between the bulk and locally available  $CO_2$  gas concentrations is predicted to be greater at lower flow rates. Tan et al.<sup>[63]</sup> discussed the same trend for  $CO_2$  local availability in  $CO_2RR$  environments at low flow rates.

As shown in Figure 8a,  $FE_{CO}$  declines from 18.3% to 7.0% when the  $CO_2$  flow rate was reduced from  $\lambda = 10.78$  to 3.01. Interestingly, an even lower FE for CO was observed under combined back pressure and low  $\lambda$  conditions (from 26.7% to 4.4%). Back pressure enhanced CO production at higher  $\lambda$ , whereas it appeared to facilitate the opposite at lower  $\lambda$ . This suggests that the surface coverage at combined back pressure and low flow rates offers an environment where  $CO^*$  does not desorb but further reacts to  $C_{2+}$  products. Lower  $\lambda$  conditions showed  $H_2$  FEs

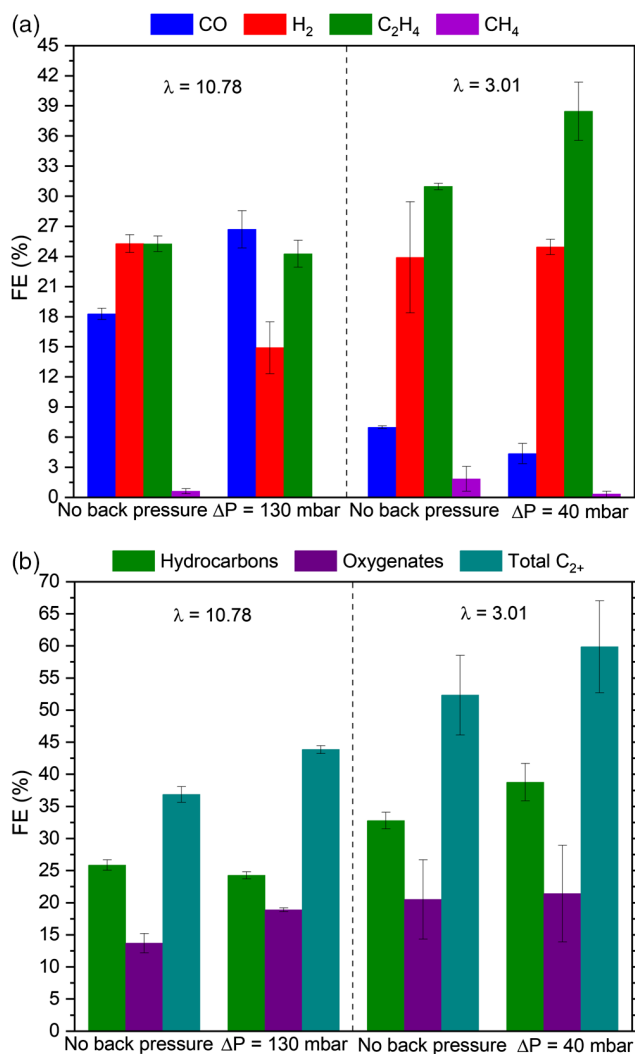


**Figure 8.** a) FEs of CO, H<sub>2</sub>, C<sub>2</sub>H<sub>4</sub> and CH<sub>4</sub> with various back pressure and flow rates at  $t = 3$  h. b) Selectivities of oxygenate, hydrocarbon and C<sub>2+</sub> products with various back pressure and flow rates at  $t = 3$  h.

similar to that of high  $\lambda$ , at the  $\approx 25\%$  range, independent of back pressure. HER was not suppressed at combined low  $\lambda$  and back pressure ( $FE_{H_2} = 25.0\%$ ) as much when compared with high  $\lambda$  and back pressure case ( $FE_{H_2} = 14.9\%$ ). The interpretations from CO and H<sub>2</sub> production signal that  $CO_2$  surface coverage reaches a smaller extent under lower flow rates, leading to lower  $CO^*$  coverage and more abundant H\*.  $FE_{CH_4}$  going up to 1.83% at low  $\lambda$  confirms that H\* availability is higher at lower flow rates.

Most interestingly, a lower  $CO^*/H^*$  coverage ratio and shorter residence time obtained by combined back pressure and low  $\lambda$  boosted C<sub>2</sub>H<sub>4</sub> production.  $FE_{C_2H_4}$  is increased from 24.3% to 38.5% when a low flow rate is used in combination with back pressure. A smaller improvement to the base case, to  $FE_{C_2H_4}$  of 31.0%, is observed at low flow rates without back pressure, this would suggest that back pressure contributes significantly to overall improvement and that the combined effects of optimum  $CO^*/H^*$  coverage and longer residence time in the catalyst layer favor C<sub>2</sub>H<sub>4</sub> formation. Together with boosted C<sub>2</sub>H<sub>4</sub>



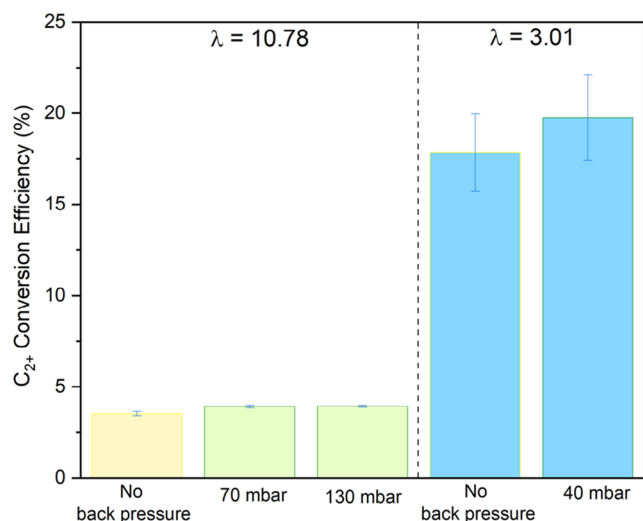


**Figure 9.** C<sub>2+</sub> conversion efficiencies at different feed flow rates and back pressures at  $t = 3$  h.

production,  $FE_{C_{2+}} = 60\%$  was achieved by combining back pressure and low flow rates, which is significantly greater than the 37% achieved in the base case (Figure 8b).

Finally, **Figure 9** shows how C<sub>2+</sub> conversion efficiency depends on feed flow rate and back pressure. A combination of low feed flow rate and back pressure delivers the highest C<sub>2+</sub> conversion efficiency at 19.8%, compared to 3.5% in the base case. Significantly lower levels of unconverted CO<sub>2</sub> at low feed flow rates and higher selectivity towards C<sub>2+</sub> with back pressure and low flow rate enable this remarkable improvement in the conversion efficiency. C<sub>2+</sub> conversion efficiency is defined in the Equation (3) in the Experimental section.

#### 4. Conclusion

CO<sub>2</sub>RR on CuO gas diffusion cathode electrodes was investigated in a flow cell environment at an applied current density of 200 mA cm<sup>-2</sup> under various back pressures and feed flow rates. Applying back pressure of 130 mbar was shown to prolong the stable operation time to 72 h ( $FE_{H_2} < 50\%$ ,  $FE_{C_{2+}} > 20\%$ ), doubling the duration observed from the base case. A high CO\* coverage due to abundant CO<sub>2</sub>\* provided by back pressure suppresses HER by blocking the active sites and/or changing the H\* binding energy. Suppressing HER increases the selectivity toward CO<sub>2</sub>RR products in addition to prolonging CO<sub>2</sub>RR stability. By differing the partial pressure of CO<sub>2</sub> at  $\Delta P = 130$  mbar, the primary reason for stability increase with back pressure application was shown to be abundant CO<sub>2</sub>\* coverage rather than decrease in the degree of electrode flooding.

Back pressure at  $\Delta P = 130$  mbar not only lowers H<sub>2</sub> production, but also enables higher production of CO and oxygenates. The ratio of oxygenates to hydrocarbons can be tuned from 0.53 to 0.85 at  $\Delta P = 0$ –130 mbar range. This enhancement in oxygenate production stems from higher selectivity toward ethanol and propanol and is suggested to be driven by the formation of \*CHCHOH intermediates under higher CO\* coverage. While

boosting stability and oxygenate selectivity, back pressure also results in a loss of CO\* by desorption and therefore high CO production, possibly due to high CO<sub>2</sub>\* coverage and short residence times in the electrode. For this reason, back pressure and low flow rates were combined to ensure a longer residence time and a more optimum CO<sub>2</sub>\* coverage for C<sub>2</sub>H<sub>4</sub> formation. This enabled a significant reduction of CO in favor of C<sub>2+</sub> products, mainly ethylene. FEs of 38.5% for ethylene and 60% for C<sub>2+</sub> and CO<sub>2</sub> conversion efficiency to C<sub>2+</sub> of 19.8% were reached. Mild CO\*/H\* coverage and long residence time in the catalyst layer are shown to be optimal for C<sub>2</sub>H<sub>4</sub> production.

In summary, we demonstrate that the method of controlling back pressure is an easily implementable option in industrial applications toward manipulating the product selectivity in upscaled Cu-based CO<sub>2</sub> electrolysis cells. Further research must be done to achieve the optimum electrode and cell design that enables a more stable operation for a possible future commercialization.

#### Supporting Information

Supporting Information is available from the Wiley Online Library or from the author.

#### Acknowledgements

The authors thank Luke Luisman and Iain Malone from Johnson Matthey Public Limited Company for supplying the CuO cathode catalyst. B.S. would like to express his gratitude to Katia Rodewald from Technical University of Munich for her support with scanning electron micrograph characterization of the electrodes, to Professor Dr. Wolfgang Eisenreich from Technical University of Munich for his support with NMR measurements, to Nemanja Martic for conducting XRD measurements, and to Dr. Remigiusz Pastusiak and Dr. Kerstin Wiesner-Fleischer for the valuable discussions and support in the laboratory. B.S. and S.L. acknowledge support from the TUM Graduate School. This research did not receive any specific grant from funding agencies in the public, commercial, or not-for-profit sectors.

Open Access funding enabled and organized by Projekt DEAL.

#### Conflict of Interest

The authors declare no conflict of interest.

#### Data Availability Statement

The data that support the findings of this study are available in the supplementary material of this article.

#### Keywords

CO<sub>2</sub>, CO<sub>2</sub> electrolysis, CO<sub>2</sub>RR, commercialization, gas diffusion electrodes pressure, selectivity, stability

Received: August 20, 2022

Revised: October 6, 2022

Published online: October 21, 2022

- [1] Y. Hori, K. Kikuchi, A. Murata, S. Suzuki, *Chem. Lett.* **1986**, *15*, 897.
- [2] N. Martić, C. Reller, C. Macauley, M. Löffler, A. M. Reichert, T. Reichbauer, K.-M. Vetter, B. Schmid, D. McLaughlin, P. Leidinger, D. Reinisch, C. Vogl, K. J. J. Mayrhofer, I. Katsounaros, G. Schmid, *Energy Environ. Sci.* **2020**, *13*, 2993.
- [3] L. Wang, S. A. Nitopi, E. Bertheussen, M. Orazov, C. G. Morales-Guio, X. Liu, D. C. Higgins, K. Chan, J. K. Nørskov, C. Hahn, T. F. Jaramillo, *ACS Catal.* **2018**, *8*, 7445.
- [4] Y. Hori, in *Modern Aspects of Electrochemistry* (Eds: C. G. Vayenas, R. E. White, M. E. Gamboa-Aldeco), Springer New York, New York, NY **2008**, pp. 89–189.
- [5] K. P. Kuhl, E. R. Cave, D. N. Abram, T. F. Jaramillo, *Energy Environ. Sci.* **2012**, *5*, 7050.
- [6] A. A. Peterson, F. Abild-Pedersen, F. Studt, J. Rossmeisl, J. K. Nørskov, *Energy Environ. Sci.* **2010**, *3*, 1311.
- [7] A. Bagger, W. Ju, A. S. Varela, P. Strasser, J. Rossmeisl, *Chemphyschem* **2017**, *18*, 3266.
- [8] S. Nitopi, E. Bertheussen, S. B. Scott, X. Liu, A. K. Engstfeld, S. Horch, B. Seger, I. E. L. Stephens, K. Chan, C. Hahn, J. K. Nørskov, T. F. Jaramillo, I. Chorkendorff, *Chem. Rev.* **2019**, *119*, 7610.
- [9] K. Jiang, R. B. Sandberg, A. J. Akey, X. Liu, D. C. Bell, J. K. Nørskov, K. Chan, H. Wang, *Nat. Catal.* **2018**, *1*, 111.
- [10] Y. Lum, J. W. Ager, *Energy Environ. Sci.* **2018**, *11*, 2935.
- [11] K. D. Yang, W. R. Ko, J. H. Lee, S. J. Kim, H. Lee, M. H. Lee, K. T. Nam, *Angew. Chem. Int. Ed.* **2017**, *56*, 796.
- [12] W. Tang, A. A. Peterson, A. S. Varela, Z. P. Jovanov, L. Bech, W. J. Durand, S. Dahl, J. K. Nørskov, I. Chorkendorff, *Phys. Chem. Chem. Phys.* **2012**, *14*, 76.
- [13] M. R. Gonçalves, A. Gomes, J. Condeço, T. Fernandes, T. Pardal, C. Sequeira, J. B. Branco, *Electrochim. Acta* **2013**, *102*, 388.
- [14] H. Mistry, A. S. Varela, C. S. Bonifacio, I. Zegkinoglou, I. Sinev, Y.-W. Choi, K. Kisslinger, E. A. Stach, J. C. Yang, P. Strasser, B. R. Cuenya, *Nat. Commun.* **2016**, *7*, 12123.
- [15] C. W. Li, J. Ciston, M. W. Kanan, *Nature* **2014**, *508*, 504.
- [16] N. Martić, C. Reller, C. Macauley, M. Löffler, B. Schmid, D. Reinisch, E. Volkova, A. Maltenberger, A. Rucki, K. J. J. Mayrhofer, G. Schmid, *Adv. Energy Mater.* **2019**, *9*, 1901228.
- [17] Y. Wang, Z. Wang, C.-T. Dinh, J. Li, A. Ozden, M. Golam Kibria, A. Seifitokaldani, C.-S. Tan, C. M. Gabardo, M. Luo, H. Zhou, F. Li, Y. Lum, C. McCallum, Y. Xu, M. Liu, A. Proppe, A. Johnston, P. Todorovic, T.-T. Zhuang, D. Sinton, S. O. Kelley, E. H. Sargent, *Nat. Catal.* **2020**, *3*, 98.
- [18] G. L. de Gregorio, T. Burdyny, A. Loiudice, P. Iyengar, W. A. Smith, R. Buonsanti, *ACS Catal.* **2020**, *10*, 4854.
- [19] E. Bertheussen, T. V. Hogg, Y. Abghoui, A. K. Engstfeld, I. Chorkendorff, I. E. L. Stephens, *ACS Energy Lett.* **2018**, *3*, 634.
- [20] C. Chen, Y. Li, S. Yu, S. Louisia, J. Jin, M. Li, M. B. Ross, P. Yang, *Joule* **2020**, *4*, 1688.
- [21] S. Lee, G. Park, J. Lee, *ACS Catal.* **2017**, *7*, 8594.
- [22] Y. Zhou, F. Che, M. Liu, C. Zou, Z. Liang, P. de Luna, H. Yuan, J. Li, Z. Wang, H. Xie, H. Li, P. Chen, E. Bladt, R. Quintero-Bermudez, T.-K. Sham, S. Bals, J. Hofkens, D. Sinton, G. Chen, E. H. Sargent, *Nat. Chem.* **2018**, *10*, 974.
- [23] F. P. García de Arquer, C.-T. Dinh, A. Ozden, J. Wicks, C. McCallum, A. R. Kirmani, D.-H. Nam, C. Gabardo, A. Seifitokaldani, X. Wang, Y. C. Li, F. Li, J. Edwards, L. J. Richter, S. J. Thorpe, D. Sinton, E. H. Sargent, *Science* **2020**, *367*, 661.
- [24] E. W. Lees, B. A. W. Mowbray, D. A. Salvatore, G. L. Simpson, D. J. Dvorak, S. Ren, J. Chau, K. L. Milton, C. P. Berlinguette, *J. Mater. Chem. A* **2020**, *8*, 19493.
- [25] S. Hernandez-Aldave, E. Andreoli, *Catalysts* **2020**, *10*, 713.
- [26] D. Higgins, C. Hahn, C. Xiang, T. F. Jaramillo, A. Z. Weber, *ACS Energy Lett.* **2019**, *4*, 317.
- [27] X. Wang, J. F. de Araújo, W. Ju, A. Bagger, H. Schmies, S. Kühl, J. Rossmeisl, P. Strasser, *Nat. Nanotechnol.* **2019**, *14*, 1063.
- [28] Y. Hori, R. Takahashi, Y. Yoshinami, A. Murata, *J. Phys. Chem. B* **1997**, *101*, 7075.
- [29] T. Cheng, H. Xiao, W. A. Goddard, *Proc. Natl. Acad. Sci. U.S.A.* **2017**, *114*, 1795.
- [30] Y. Hori, A. Murata, R. Takahashi, *J. Chem. Soc., Faraday Trans. 1* **1989**, *85*, 2309.
- [31] D. W. DeWulf, T. Jin, A. J. Bard, *J. Electrochem. Soc.* **1989**, *136*, 1686.
- [32] Y. Hori, A. Murata, R. Takahashi, S. Suzuki, *J. Am. Chem. Soc.* **1987**, *109*, 5022.
- [33] D.-H. Nam, P. de Luna, A. Rosas-Hernández, A. Thevenon, F. Li, T. Agapie, J. C. Peters, O. Shekhah, M. Eddaoudi, E. H. Sargent, *Nat. Mater.* **2020**, *19*, 266.
- [34] S. Ma, M. Sadakiyo, R. Luo, M. Heima, M. Yamauchi, P. J. Kenis, *J. Power Sources* **2016**, *301*, 219.
- [35] K. P. Kuhl, T. Hatsukade, E. R. Cave, D. N. Abram, J. Kibsgaard, T. F. Jaramillo, *J. Am. Chem. Soc.* **2014**, *136*, 14107.
- [36] R. Kas, R. Kortlever, H. Yilmaz, M. T. M. Koper, G. Mul, *Chemoelectrochem* **2015**, *2*, 354.
- [37] X. Liu, P. Schlexer, J. Xiao, Y. Ji, L. Wang, R. B. Sandberg, M. Tang, K. S. Brown, H. Peng, S. Ringe, C. Hahn, T. F. Jaramillo, J. K. Nørskov, K. Chan, *Nat. Commun.* **2019**, *10*, 32.
- [38] Y. Lum, T. Cheng, W. A. Goddard, J. W. Ager, *J. Am. Chem. Soc.* **2018**, *140*, 9337.
- [39] I. Ledezma-Yanez, E. P. Gallent, M. T. Koper, F. Calle-Vallejo, *Catal. Today* **2016**, *262*, 90.
- [40] E. Bertheussen, A. Verdaguer-Casadevall, D. Ravasio, J. H. Montoya, D. B. Trimarco, C. Roy, S. Meier, J. Wendland, J. K. Nørskov, I. E. L. Stephens, I. Chorkendorff, *Angew. Chem., Int. Ed.* **2016**, *55*, 1450.
- [41] E. L. Clark, A. T. Bell, *J. Am. Chem. Soc.* **2018**, *140*, 7012.
- [42] Y. Y. Birdja, M. T. M. Koper, *J. Am. Chem. Soc.* **2017**, *139*, 2030.
- [43] M. Rahaman, A. Dutta, A. Zanetti, P. Broekmann, *ACS Catal.* **2017**, *7*, 7946.
- [44] D. Ren, N. T. Wong, A. D. Handoko, Y. Huang, B. S. Yeo, *J. Phys. Chem. Lett.* **2016**, *7*, 20.
- [45] N. S. Romero Cuellar, K. Wiesner-Fleischer, M. Fleischer, A. Rucki, O. Hinrichsen, *Electrochim. Acta* **2019**, *307*, 164.
- [46] J. Li, Z. Wang, C. McCallum, Y. Xu, F. Li, Y. Wang, C. M. Gabardo, C.-T. Dinh, T.-T. Zhuang, L. Wang, J. Y. Howe, Y. Ren, E. H. Sargent, D. Sinton, *Nat. Catal.* **2019**, *2*, 1124.
- [47] M. Löffler, P. Khanipour, N. Kulyk, K. J. Mayrhofer, I. Katsounaros, *ACS Catal.* **2020**, *10*, 6735.
- [48] R. Kortlever, J. Shen, K. J. P. Schouten, F. Calle-Vallejo, M. T. M. Koper, *J. Phys. Chem. Lett.* **2015**, *6*, 4073.
- [49] X. Feng, K. Jiang, S. Fan, M. W. Kanan, *ACS Cent. Sci.* **2016**, *2*, 169.
- [50] A. Verdaguer-Casadevall, C. W. Li, T. P. Johansson, S. B. Scott, J. T. McKeown, M. Kumar, I. E. L. Stephens, M. W. Kanan, I. Chorkendorff, *J. Am. Chem. Soc.* **2015**, *137*, 9808.
- [51] C. Hahn, T. Hatsukade, Y.-G. Kim, A. Vailionis, J. H. Baricuatro, D. C. Higgins, S. A. Nitopi, M. P. Soriaga, T. F. Jaramillo, *Proc. Natl. Acad. Sci. U.S.A.* **2017**, *114*, 5918.
- [52] Y.-G. Kim, A. Javier, J. H. Baricuatro, M. P. Soriaga, *Electrocatalysis* **2016**, *7*, 391.
- [53] Y. Hori, H. Konishi, T. Futamura, A. Murata, O. Koga, H. Sakurai, K. Oguma, *Electrochim. Acta* **2005**, *50*, 5354.
- [54] J.-F. Xie, Y.-X. Huang, W.-W. Li, X.-N. Song, L. Xiong, H.-Q. Yu, *Electrochim. Acta* **2014**, *139*, 137.
- [55] J. Lee, Y. Tak, *Electrochim. Acta* **2001**, *46*, 3015.
- [56] G. Kyriacou, A. Anagnostopoulos, *J. Electroanal. Chem.* **1992**, *322*, 233.

- [57] X. Nie, M. R. Esopi, M. J. Janik, A. Asthagiri, *Angew. Chem. Int. Ed.* **2013**, *52*, 2459.
- [58] S. A. Akhade, W. Luo, X. Nie, N. J. Bernstein, A. Asthagiri, M. J. Janik, *Phys. Chem. Chem. Phys.* **2014**, *16*, 20429.
- [59] W. T. Osowiecki, J. J. Nussbaum, G. A. Kamat, G. Katsoukis, M. Ledendecker, H. Frei, A. T. Bell, A. P. Alivisatos, *ACS Appl. Energy Mater.* **2019**, *2*, 7744.
- [60] L.-C. Weng, A. T. Bell, A. Z. Weber, *Phys. Chem. Chem. Phys.* **2018**, *20*, 16973.
- [61] M. Leonard, M. Orella, N. Aiello, Y. Román-Leshkov, A. Forner-Cuenca, F. Brushett, *Flooded by Success: On the Role of Electrode Wettability in CO<sub>2</sub> Electrolyzers that Generate Liquid Products*, IOP, Bristol, England **2020**.
- [62] M. E. Leonard, L. E. Clarke, A. Forner-Cuenca, S. M. Brown, F. R. Brushett, *ChemSusChem* **2020**, *13*, 400.
- [63] Y. C. Tan, K. B. Lee, H. Song, J. Oh, *Joule* **2020**, *4*, 1104.
- [64] C. Kim, L.-C. Weng, A. T. Bell, *ACS Catal.* **2020**, *10*, 12403.
- [65] C. Kim, J. C. Bui, X. Luo, J. K. Cooper, A. Kusoglu, A. Z. Weber, A. T. Bell, *Nat. Energy* **2021**, *6*, 1026.
- [66] Y. Hori, A. Murata, Y. Yoshinami, *J. Chem. Soc., Faraday Trans.* **1991**, *87*, 125.
- [67] H. Ooka, M. C. Figueiredo, M. T. M. Koper, *Langmuir* **2017**, *33*, 9307.
- [68] R. B. Sandberg, J. H. Montoya, K. Chan, J. K. Nørskov, *Surf. Sci.* **2016**, *654*, 56.
- [69] M. Moradzaman, C. S. Martínez, G. Mul, *Sustainable Energy Fuels* **2020**, *4*, 5195.